ChemComm
Chemical Communications

Accepted Manuscript

This article can be cited before page numbers have been issued, to do this please use: M. Mukoyoshi and H. Kitagawa, *Chem. Commun.*, 2022, DOI: 10.1039/D2CC03233C.

ROYAL SOCIETY OF CHEMISTRY

rsc.li/chemcomm

View Article Online
DOI: 10.1039/D2CC03233C

FEATURE ARTICLE

Nanoparticle/metal–organic framework hybrid catalysts: elucidating the role of the MOF

Megumi Mukoyoshi* and Hiroshi Kitagawa*

Received 00th January 20xx,
Accepted 00th January 20xx

DOI: 10.1039/x0xx00000x

Hybrid materials of metal–organic frameworks (MOFs) and nanoparticles (NPs) have attracted significant attention because of the wide variety of attractive properties derived from the two components. In the last decade, the development of synthesis techniques for NP/MOF composites was particularly significant. In the field of catalysis in particular, various synergistic effects that make the composites attractive catalysts have been reported. However, the role of MOFs in the composite catalysts is still not well understood and is being elucidated. In this feature article, we focus on recent progress on NP/MOF composite catalysts, concentrating on the analysis of the interaction between NPs and MOFs and the reaction mechanisms, together with the synthetic techniques used for NP/MOF hybrid materials.

1. Introduction

Metal–organic frameworks (MOFs),[1–3] also known as porous coordination polymers (PCPs), are a new class of crystalline porous materials constructed from metal ions and organic linkers. Because of their highly regular pores and large surface areas, they have attracted much attention for their potential uses, such as gas storage,[4] separation,[5] catalysis,[6] and ion conduction.[7] In recent years, research has been conducted into further expanding their functionality by hybridizing MOFs with various materials, such as organic molecules, enzymes, polymers, metal nanoparticles (NPs), and polyoxometalates.[8–10] In addition to simply combining MOFs with other functional materials, MOF derivatives such as MOF-derived carbon materials[11] and single-atom catalysts[12] are also well exploited. In particular, hybrid materials composed of MOFs and NPs (NP/MOF, or NP@MOF composites) are being intensively studied as efficient catalysts because of their chemical and physical properties. Generally, to prevent the NPs from aggregating and to maximize the use of their surface, porous materials such as zeolite[13] and porous carbon[14] are used as support materials for the NPs in catalysis. The support materials themselves are often inert, and even in composites with MOFs, most early examples simply added NP functionality to the MOF.[15,16] However, MOF properties that are not found in other porous materials, such as high designability, wide variety, and

Division of Chemistry, Graduate School of Science, Kyoto University, Kitashirakawa-Oiwakecho, Sakyo-ku, Kyoto 606-8502, Japan.
E-mail: mukoyoshi@ssc.kuchem.kyoto-u.ac.jp, kitagawa@kuchem.kyoto-u.ac.jp

Megumi Mukoyoshi

Megumi Mukoyoshi graduated from Kyoto University in 2014 with MSc in Chemistry), after which she worked as a researcher at Showa Denko K. K. (2014-2017) and Daikin Industries, Ltd. (2018-2021), where she worked on catalyst development in chemical plants and on gas separators using MOFs. She returned to Kyoto University and obtained her PhD in 2022. In April 2022, she was appointed Assistant Professor at Kyoto University. Her current research focuses on the design of advanced functional metal nanoparticles, MOFs, and their hybrid materials.

Hiroshi Kitagawa

Hiroshi Kitagawa completed his PhD at Kyoto University in 1991. After working as Assistant Professor at the Institute for Molecular Science(IMS) and Japan Advanced Institute of Science and Technology (JAIST), he was appointed Associate Professor at the University of Tsukuba in 2000. He became Professor of Chemistry at Kyushu University in 2003 and moved to Kyoto University as Professor in 2009. He is also engaged at JST as Director of the network-type research institution "Exploring Innovative Materials in Unknown Search Space", CREST. He has published more than 460 original research papers dealing with solid-state chemistry, coordination chemistry, nanoscience, low-dimensional electron systems, and molecule-based conductors.

selective sorption, are expected to provide synergistic effects as novel efficient catalysts.

By combining MOFs with NPs, various MOF functions can be expected to contribute to more efficient catalytic reactions. For example, the MOF pores can act as molecular sieves; the composite catalysts can be designed so that only gas molecules necessary for the reaction are captured and are efficiently delivered to the NP surface, where the catalytic reaction occurs. The regular pores in MOFs can also be used to capture the reactant molecules at high density, and pseudo high-pressure microenvironments are expected to be achieved to enhance reaction efficiency. In addition, it is well known that catalytic properties such as activity or selectivity strongly depend on the electronic states of NPs interacting with support materials. From this viewpoint, MOFs are attractive materials as well because their electronic properties can be finely controlled by using tuning methods such as ligand substitution or defect introduction. These synergistic effects can now be confirmed due to the development of synthetic techniques that allow precise control of the structure of the composite catalysts. However, in actual cases, it is difficult to analyse the role of the MOFs in the composite catalysts, because multiple effects often occur simultaneously. To date, the presence of these effects has been continually suggested, but elucidation of the reaction mechanism is still in its infancy. In this review article, first, the synthetic techniques of NP/MOF composite catalysts are briefly introduced; then, recent progress is reviewed, together with analyses of the interaction between NPs and MOFs, with the main focus on reaction mechanisms.

2. Synthesis methods for NP/MOF composites

Various methods for hybridizing NPs and MOFs have been explored to date, and these are classified into several types (Fig. 1). The first is called the "bottle-around-ship" approach, in which NPs are introduced into prepared MOFs.[17] Examples include the solid grinding, solution impregnation, and chemical vapor deposition (CVD) methods. In addition, the self-template method, hybridizing MOFs with NPs generated from the MOFs themselves is also classified as belonging to this approach.[18] The second type is hybridization with a MOF on prepared NPs, such as the encapsulation method ("ship-in-a-bottle" approach[19]). A third approach is the one-step method,[20] which includes simultaneous synthesis of the two components to afford NP/MOF hybrid materials. Solid grinding method was used in early studies, followed by the development of solution impregnation, CVD, and encapsulation methods to precisely control the size and loading position of NPs. Self-template method and one-pot method were also proposed as simple preparation methods for NP/MOF composite materials. Currently, solution impregnation method and encapsulation method are most commonly as facile and controllable approach.

2.1. Introducing NPs into prepared MOFs

2.1.1. Solid grinding method. In early examples, NPs were deposited on MOFs by simple mixing of the MOF and metal precursor by solid grinding, and the metal NPs were synthesized by reduction of the metal precursor. By using the solid grinding method, Haruta and co-workers embedded Au NPs on various MOFs, such as MIL-53(Al), MOF-5, HKUST-1, ZIF-8, CPL-1, and CPL-2.[16,21] The metal precursor was the volatile organogold complex, $(CH_3)_2Au(acac)$ (acac = acetylacetonate), and it was reduced by treatment in H_2. This technique was often used in early attempts to develop NP/MOF composites because of its simplicity and because of the small amount of solvent required. By contrast, due to the need to use volatile metal precursors, the number of reported cases using this method in recent years is small; likewise, this also applies to the CVD method, which will be discussed later.

2.1.2. Solution impregnation method. The solution impregnation method is another simple means of NP/MOF

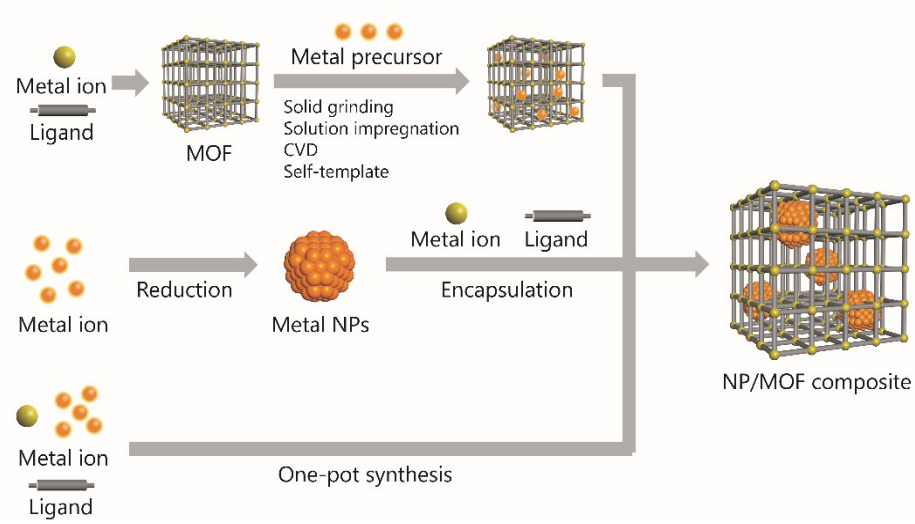

Fig. 1 Schematic illustration of synthesis methods of NP/MOF composites. (a) Introduction of NPs into prepared MOFs ("bottle-around-ship" approach). (b) Hybridization with a MOF on prepared NPs ("ship-in-a-bottle" approach). (c) One-step method, with simultaneous synthesis of NPs and MOFs to afford NP/MOF hybrid materials.

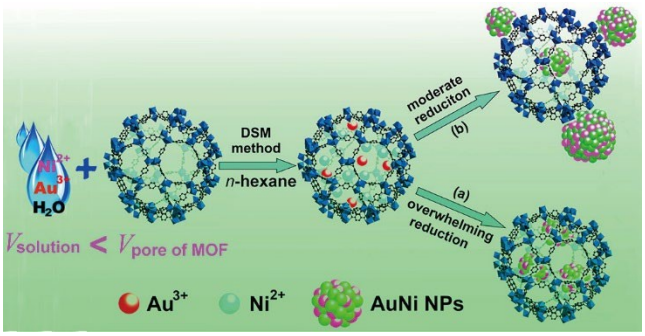

Fig. 2 Schematic illustration showing immobilization of AuNi NPs into MIL-101 using the double-solvent method (DSM). Reprinted with permission from Ref 26. Copyright 2013 American Chemical Society.

composite fabrication. In this technique, a metal precursor solution is embedded into the MOF pores and is reduced by H_2 or $NaBH_4$. Solution impregnation methods are applied to synthesize not only monometallic NPs (Ag,[22] Rh,[23] Pd, and Cu[24]), but also alloy NPs including Pd/Cu,[24] Ni/Pt,[25] and Au/Ni.[26] In addition, NPs that have been already synthesized can be dispersed in solution and loaded onto MOFs.[27] This technique can be applied to various metal precursors and NPs, and is still intensively used to fabricate composite catalysts. Although this is a versatile and effective way to hybridize MOFs with NPs, it is difficult to precisely control the position of NPs (on/in the host MOFs). To solve this problem, a double-solvent method (DSM) was developed by Aijaz *et al.*[28] In the double-solvent method, the hydrophilic/hydrophobic nature of the MOF cavities is used to introduce the metal precursor only into the pore, preventing aggregation of NPs on the MOF surface. Aijaz *et al*. used MIL-101, $Cr_3F(H_2O)_2O[(O_2C)C_6H_4(CO_2)]_3$, the pores of which are known to be hydrophilic, as the NP host. Because the hydrophilic environment of the MIL-101 pores, the water-dissolved metal precursor H_2PtCl_6 can easily penetrate the MOF. The deposition of the metal precursor on the outer surface is prevented by dispersing the MOF in a hydrophobic solvent (hexane). Pt NPs with a size of 1.8 ± 0.2 nm immobilized inside the pores of MIL-101 were obtained by heating the precursor in a H_2 atmosphere. The authors also successfully introduced well-dispersed AuNi alloy NPs into the pores of MIL-101, and the composite catalysts exhibited high activity for hydrogen generation reaction from ammonia borane (Fig. 2).[26]

2.1.3. CVD method. To control the NP size and embed NPs inside the MOF, a CVD method has been developed.[15,29] The host MOF is loaded with a metal precursor in the vapor phase, followed by decomposition and/or reduction to obtain NPs within the pores of the MOF. The first study on the CVD method was performed by Fischer *et al*. in 2005 by using MOF-5.[15] They successfully fabricated Au, Cu, and Pd NP/MOF composites by using $(CH_3)Au(PMe_3)$, $(\eta^5\text{-}C_5H_5)Cu(PMe_3)$, and $(\eta^3\text{-}C_3H_5)Pd(\eta^5\text{-}C_5H_5)$ as the organometallic precursors, respectively. This CVD method has the advantage of controlling the size of the resultant nanoparticles, but it requires a complicated process and is not considered to be suitable for large-scale production.

2.1.4. Self-template method. Because MOFs are composed of metal ions and organic ligands, metal NPs can be generated from metal ions in the MOF. This approach provides simple methods to obtain NP/MOF composites because no additional metal precursors are needed. NPs are generally obtained by partial decomposition using a thermal treatment[30] or a reduction reaction.[31] Mukoyoshi *et al*. reported a facile synthetic method of Ni NP/MOF-74 hybrid materials by simply heating Ni-MOF-74, Ni_2(dhtp) (H_4dhtp = 2,5-dihydroxyterephthalic acid).[30] In this method, the functionalized hydroquinone ligand, H_4dhtp, may act as a reducing agent for Ni ions and generate Ni NPs inside the MOF. Recently, Fu *et al*. fabricated well-dispersed metal NPs embedded in MOFs by slow chemical reduction of MOF precursors. This synthesis method can proceed at room temperature by using $NaBH_4$ as a reducing agent.[31] In general, it is impossible to introduce NPs composed of a different type of metal than the constituent elements of the host MOF using these self-template methods; however, the design of appropriate ligands makes this possible. Chen *et al*. achieved Pd NPs inside MOF cavities by introducing Pd precursors prior to MOF assembly.[32]

2.2. Hybridization with MOFs on prepared NPs

2.2.1. Encapsulation method. NP/MOF composites are also synthesized by encapsulating protecting agent-stabilized NPs in MOFs.[19,33–35] MOFs synthesis and NP incorporation into MOFs proceeded simultaneously by introducing NPs in a precursor solution of organic ligands and metal salts. Lu *et al*. demonstrated encapsulation of various nanoparticles within ZIF-8, in a controllable way.[34] They prepared various poly-vinylpyrrolidone (PVP)-capped NPs, such as Au, Ag, Pt, CdTe, Fe_3O_4, and lanthanide-doped $NaYF_4$, and successfully embedded them into ZIF-8 crystals. Moreover, the NP spatial distribution within ZIF-8 can be controlled by adjusting the time of NP addition during the MOF-formation reactions. Possible drawbacks of this method are that any protecting agents and/or surfactants used to stabilize the NPs are incorporated as impurities, which may have a negative effect on the catalytic properties of the NPs. Recently, Li *et al*. developed a novel

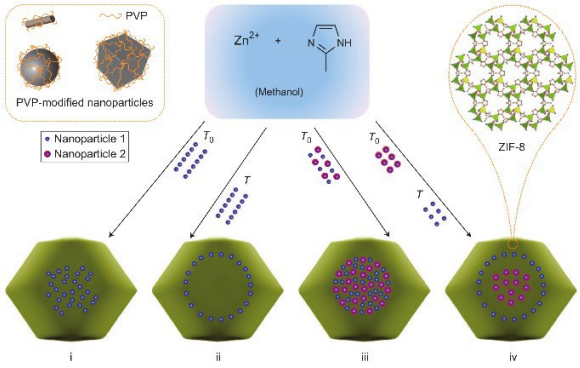

Fig. 3 Synthetic scheme of NPs encapsulated in ZIF-8 with controlled positions. Reproduced from Ref. 34 with permission from Nature Publishing Group, copyright 2012.

View Article Online
DOI: 10.1039/D2CC03233C

strategy to achieve a direct contact between NPs and MOFs.[36] A weakly adsorbed capping agent, cetyltrimethylammonium bromide (CTAB) was used to synthesize NPs and CATB was confirmed to be replaced by MOFs. The authors successfully synthesized NP@MOF materials and confirmed that a high selectivity of the desired products was achieved by generating a direct interface in Au NP@MOF catalysts.

In encapsulation methods, metal oxides are often used as intermediates for subsequent MOF growth. For example, Tsung and co-workers generated yolk-shell Pd NP@ZIF-8 catalysts using a Cu_2O layer as the sacrificial template.[37] At first, pre-synthesized Pd NPs are coated with Cu_2O, and polycrystalline ZIF-8 is synthesized around Pd@Cu_2O by mixing with the ZIF-8 precursors, 2-methylimidazole (2-meIm) and zinc nitrate in methanol. The Cu_2O is etched off simultaneously with the ZIF-8 formation, due to the low pH of the solution (pH = 5) derived from the deprotonation of 2-meIm. Because MOFs can be synthesized not only by the solvothermal method but also by the mechanochemical method,[38,39] NP encapsulation in the MOFs can also be conducted via the mechanochemical process. In 2019, Pd@ZIF-8 composites were prepared by a mechanochemistry-assisted encapsulation method.[40] ZnO was used as the metal precursor of ZIF-8, which directly mixed ZnO with $PdCl_2$, the metal precursor of Pd NPs. Pd NPs supported on the ZnO (Pd/ZnO) are formed by reduction in H_2 following ball milling. Pd@ZIF-8 was synthesized by ball milling of the as-prepared Pd/ZnO with 2-meIm, where ZnO reacted and transformed into ZIF-8. The significant advantage of this technique is its suitability for large-scale synthesis, which is promising for practical use.

2.3. One-pot method

The two preparation techniques for NP/MOF composites described so far require at least two or more steps, and there was a need for further development of simpler hybridization methods. A facile one-pot method to prepare NP@MOF composites was first reported by Tang *et al*. in 2013.[20] They found that Au@MOF-5 materials can be directly obtained by mixing the precursors of the Au NPs and MOF ($HAuCl_4$, zinc nitrate, and 1,4-benzenedicarboxylate) in the reaction solution. Au NPs are first synthesized within a very short time during solution heating, and subsequently MOF-5 grows on Au NPs' surface. By using the same technique, they also successfully synthesized the Au@ZIF-8, Au@IRMOF-3, and Ag@MOF-5 composites. This one-pot method is versatile and has been applied not only to solution synthesis but also to the microwave[41] and spray-drying methods.[42]

3. Catalytic properties and reaction mechanisms of NP/MOF composites

There are several promising effects of hybridized MOF and NPs on the catalytic reaction, namely: (1) molecular sieving effects for reactant and/or product molecules (Fig.4a) ; (2) interactions between reactant molecules and MOFs within the pores of MOFs, such as condensation and diffusion effects, and conversion of reactant molecules (Fig.4b) ; and (3) electronic interactions between NPs and MOFs (Fig. 4c). In many cases, the active site of the reaction is the NP surface, and MOFs contribute to activating reactants or tuning the properties of reaction sites. For example, Yaghi and co-workers showed that Pt NP-embedded MOF nanocrystals (Pt/UiO-66) are ideal materials for changing the chemical environment of a catalyst.[43] They prepared two isoreticular MOFs with different functional groups as hosts for Pt NPs, and confirmed that these chemical environments alter the selectivity and activity in the gas-phase catalytic reaction of methylcyclopentane (MCP). Although a few hypotheses have been proposed regarding the effects of functional groups of ligands on the reaction, a detailed analysis of the reaction mechanism is still to be explored.

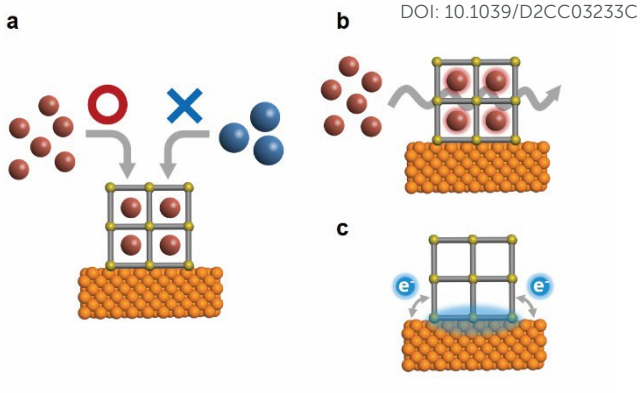

Fig. 4 Schematic illustrations showing effects to hybridized MOF and NPs on catalytic reaction. (a) Molecular sieving effects. (b) Interactions between reactant molecules and MOFs within MOF pores, such as condensation and diffusion effects, and conversion of reactant molecules. (c) Electronic interactions between NPs and MOFs.

3.1. Molecular sieving effect

MOFs have regular cavities of the same size, and molecules larger than the aperture of the MOF cavities cannot access the surface of the NPs encapsulated within the MOF. This "molecular sieving effect" can be used to select the type of molecule that reaches the NP surface, the active site, resulting in improved catalytic performance of the NP/MOF composites. Zhang *et al*. confirmed the selective molecular sieving effect of UiO-66, [$Zr_6O_4(OH)_4(BDC)_6$, BDC = 1,4-benzenedicarboxylate],[44] on Pt NPs in both gas- and liquid-phase catalytic reactions.[45] They tested various olefin hydrogenation reactions with different reactant sizes (hex-1-ene, cyclooctene, *trans*-stilbene, *cis*-stilbene, triphenyl ethylene, and tetraphenyl ethylene) on composite catalysts and compared the results with those obtained using Pt NPs supported on carbon nanotubes (Pt-CNT). It was found that the conversion rate decreased as the size of the reactant molecule increased, whereas Pt-CNT showed indiscriminating activity towards olefin hydrogenation (hex-1-ene 100%, cyclooctene 100%, *cis*-stilbene 100%, *trans*-stilbene 100%, triphenyl ethylene 89%, and tetraphenyl ethylene 18%)

View Article Online
DOI: 10.1039/D2CC03233C

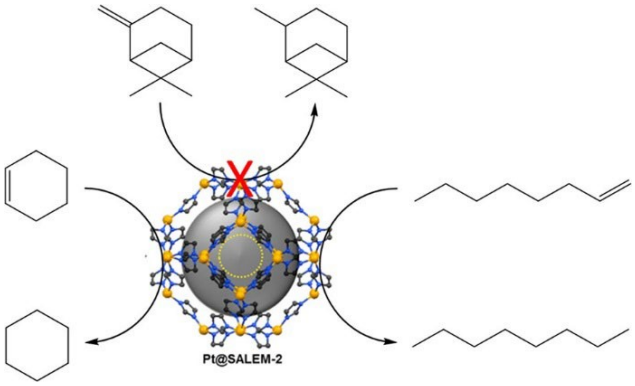

Fig. 5 Schematic illustration showing molecular sieving effects over the Pt@SALEM-2 composite catalyst. Reprinted with permission from Ref 46. Copyright 2016 American Chemical Society.

This effect can be precisely controlled as the MOF cavity size can be tuned easily by substituting the MOF ligands. Stephenson *et al*. developed the solvent-assisted linker exchange (SALE) technique to control the pore size of NP@MOF catalysts.[46] The initially synthesized Pt@ZIF-8 composite was converted to Pt@SALEM-2 by exchanging 2-meIm for imidazolate. The substitution of the ligands was confirmed by powder X-ray diffraction, ^{1}H NMR spectroscopy, inductively coupled plasma atomic-emission spectroscopy, and scanning transmission electron microscopy (STEM). They observed changes in the catalytic results corresponding to the larger aperture size resulting from ligand substitution (Fig. 5). In addition to pore size, flexibility also affects the type of reactant molecules incorporated, as shown by Chen *et al*.[47] They used two different MOFs, ZIF-8 [$Zn(mIM)_2$, mIM = 2-methyl imidazole] with a flexible structure[48] and ZIF-71 [$Zn(DClIM)_2$, DClIM = 4,5-dichloroimidazole] with a rigid structure[49] as support materials for Pt NPs. Both composite catalysts, Pt@ZIF-8 and Pt@ZIF-71, showed high catalytic activity for the selective hydrogenation of cinnamaldehyde (CAL) under mild conditions. However, the Pt@ZIF-71 composite catalysts showed lower catalytic activity and higher selectivity due to the rigid structure of ZIF-71. The high selectivity is achieved because the orientation of CAL molecules on the of the Pt NPs is fixed within the ZIF-71 pores. To date, molecular sieving effects have been observed in numerous NP/MOF composite catalysts.[34,37,50]

3.2. Interactions between reactant molecules and MOFs within MOF pores

MOFs have regular pores that can selectively adsorb gas molecules and are considered to have condensation effects. For example, a quasi-condensed CO_2 liquid phase was observed even at 1 bar and 298 K at the interface between MOF and Ag NPs.[51] Because pseudo high-pressure microenvironments can be generated by encapsulating NPs in MOFs, MOFs are expected to promote NP catalytic reactions. In addition to catalytic activity, NP reaction selectivity can be also controlled by using hybridization with MOFs. Na *et al.* found that Pt NPs embedded in UiO-66 present unusual product selectivity in hydrogenative conversion of MCP.[52] They compared the

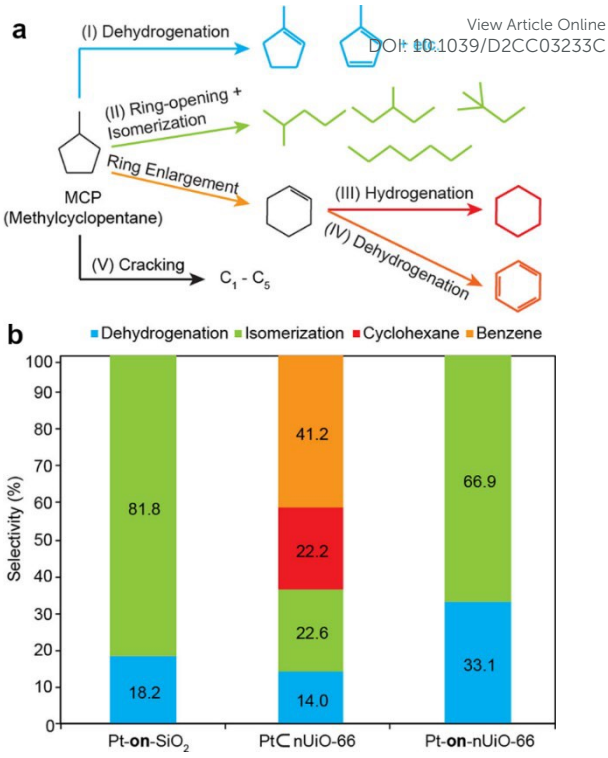

Fig. 6 (a) Schematic reaction diagram of the MCP hydrogenation reaction. (b) The results of catalytic reaction tests over three catalysts (Pt-on-SiO2, Pt⊂nUiO-66, and Pt-on-nUiO-66) obtained at 150 °C. Reprinted with permission from Ref 52. Copyright 2014 American Chemical Society.

selectivity of the Pt NP-supported surface of UiO-66 (Pt-on-nUiO-66) and embedded in UiO-66 (Pt⊂nUiO-66) and obtained different product profiles (Fig. 6). Pt⊂nUiO-66 produced C_6-cyclic hydrocarbons, whereas dehydrogenation and isomerization products were obtained by using Pt-on-nUiO-66. The difference in reaction selectivity is attributed to the increase in H_2 local concentration of H_2 inside UiO-66 pores.

Diffusion of reactant molecules is another factor that determines catalytic reaction performance as a concentration of reactant gas molecules. Because the gas diffusion rate in MOF pores is reported to be relatively slow compared with bulk gas molecules,[53] it is challenging to design NP/MOF composites with a high diffusion rate of reactant molecules. In 2017, Yang *et al*. succeeded in controlling the spatial distribution of the NPs within MOFs and achieved high catalytic activity in hydrogenation of n-hexene and cyclooctene.[54] The spatial localization of NPs can be regulated by changing the ligand concentration during the MOF encapsulation process.

In actual catalytic reactions, it is assumed that these effects occur simultaneously; however, analysis of the catalytic reaction mechanisms is difficult because of its complexity. The reactivity of gas molecules in MOF was investigated in the water–gas shift (WGS) reaction ($H_2O+CO \rightarrow H_2+CO_2$) of Pt@UiO-66 composite catalysts in 2019.[27] The activation of H_2O is the rate-limiting step of the reaction[55] and Pt NPs are well-known catalysts for the reaction. Both condensation and diffusion effects have a key role in achieving high catalytic activity,

because the concentration or flow rate of H_2O strongly affects the WGS reaction activity. To investigate the contribution of these effects, two different composite catalysts, Pt on UiO-66 and Pt@UiO-66, were synthesized. Pt on UiO-66, where Pt NPs are located on the surface of UiO-66, was prepared by the impregnation method. By contrast, Pt@UiO-66, where Pt NPs are encapsulated within UiO-66, was synthesized by mixing the pre-synthesized Pt NPs with precursors of UiO-66. In the WGS reaction tests, a higher CO conversion was observed for Pt@UiO-66 than for Pt on UiO-66 (Fig. 7). In the in situ IR spectra of the Pt@UiO-66, weak infrared (IR) bands attributed to Pt-OH species appeared, but were not observed in Pt on UiO-66. Given that Pt-OH is an active intermediate species in the WGS reaction,[56] the higher catalytic activity of Pt@UiO-66 is attributed to the presence of these intermediate species. The higher ratio of the contact interface in Pt@UiO-66 between Pt NPs and UiO-66 may promote H_2O activation. In addition, to investigate the effects of condensation and diffusion in the catalytic mechanism, the WGS reaction activity test with different H_2O flow rates was performed. Although the CO conversion of Pt@UiO-66 was higher than Pt on UiO-66 at a slow H_2O flow rate, the difference decreased with increasing flow rate and eventually the reverse tendency was observed (Fig. 8). These phenomena can be explained by competitive effects of H_2O condensation and diffusion in UiO-66 pores: when H_2O concentration is low, the condensation effect of UiO-66 has an important role to provide water molecules to the Pt NPs, with the result that Pt@UiO-66, which has a larger contact interface, showed a higher catalytic activity than Pt on UiO-66. By contrast, at higher H_2O concentration, the diffusion of water molecules into Pt NPs through UiO-66 is a dominant factor affecting the WGS reaction activity, because the condensation effect induced by UiO-66 weakens. A relatively thick (80 nm) UiO-66 shell is formed around Pt NPs, and therefore the diffusion rate of H_2O in the Pt@UiO-66 composite is believed to be slower than in Pt on UiO-66. For this reason, Pt@UiO-66 showed lower catalytic activity than Pt on UiO-66 at higher H_2O concentration. Pt NPs coated with a thinner UiO-66 layer (Pt@UiO-66-40 nm) presented a higher catalytic activity than Pt@UiO-66 and Pt on UiO-66 in the wide flow range of H_2O, supporting the authors' insights (Fig. 8).

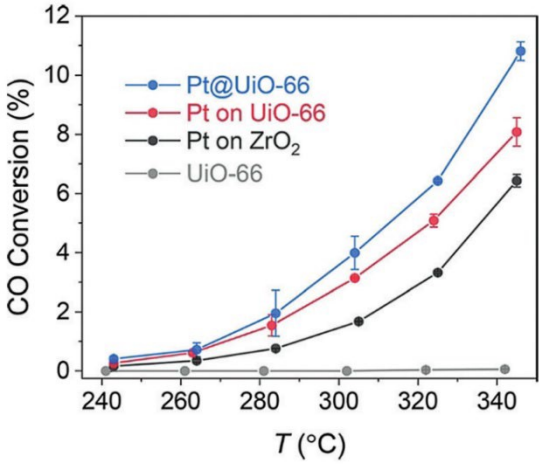

Fig. 7 Temperature dependence of CO conversion in WGS reaction. Reaction conditions: 11 sccm of H_2O, 10 sccm of CO, 50 sccm of Ar, 0.65 MPa. Reproduced with permission from Ref. 27 Copyright 2019 Wiley-VCH.

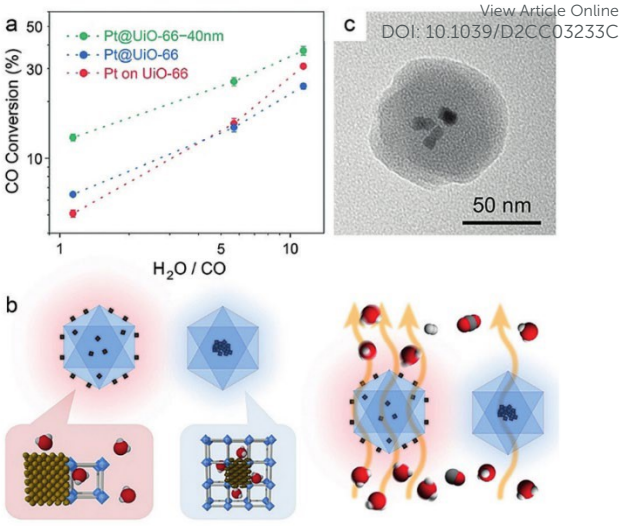

Fig. 8 (a) CO conversion versus H_2O/CO ratio in WGS reaction over Pt on UiO-66 (red), Pt@UiO-66 (blue), and Pt@UiO-66-40nm (green). Reaction conditions: 11.4, 57.0, or 114 sccm H_2O, 10 sccm CO, 50 sccm Ar, 0.65 MPa and 320°C. (b) Schematic illustrations of condensation effect (left) and diffusion effect (right) of H_2O in UiO-66 pores with Pt NPs. (c) Transmission electron microscope image of Pt@UiO-66-40nm. Reproduced with permission from Ref. 27 Copyright 2019 Wiley-VCH.

The reactivity of water molecules in the WGS reaction can also be systematically controlled through functionalization of the MOF ligands.[57] Composite catalysts composed of Pt NPs and UiO-66 or its analogues (UiO-66-H, UiO-66-Br, and UiO-66-Me_2) were synthesized and their catalytic activities in the WGS reaction were investigated. The ligand functionalization with the –Me_2 group provided a higher CO conversion than the unfunctionalized one (Pt@UiO-66-H), whereas ligand functionalization with the –Br group resulted in lower catalytic activity. From the results of solid-state NMR and in situ IR measurements, the differences in the WGS reaction activity originate from the electron density of water molecules in the UiO-66 pores. In ^{1}H NMR spectra, the chemical shifts of the adsorbed water molecules were shifted depending on the functional groups (Fig. 9a). Functionalization with the –Me_2 group, an electron-donating group, could increase the electron density of protons in the adsorbed H_2O, and vice versa. For the WGS reaction, A high electron density of H_2O is considered to be favourable for H_2O dissociation to form the active intermediate species OH.[58] The authors also confirmed that the formation of OH species resulted from H_2O activation by in situ IR spectra measurements under a reaction gas flow for three composite catalysts (Fig. 9b). The Pt–OH band intensity gradually decreases in the order Pt@UiO-66-Me_2 > Pt@UiO-66-H > Pt@UiO-66-Br, which is consistent with the WGS reactivity. Pt-OH is a known active intermediate species in the WGS

reaction,[56] and therefore, the tendency of the Pt-OH band intensity could indicate WGS catalytic activity in the Pt@UiO-66 analogues. For these reasons, Pt@UiO-66-Me$_2$ showed the highest WGS reactivity in the three Pt@UiO-66 analogues.

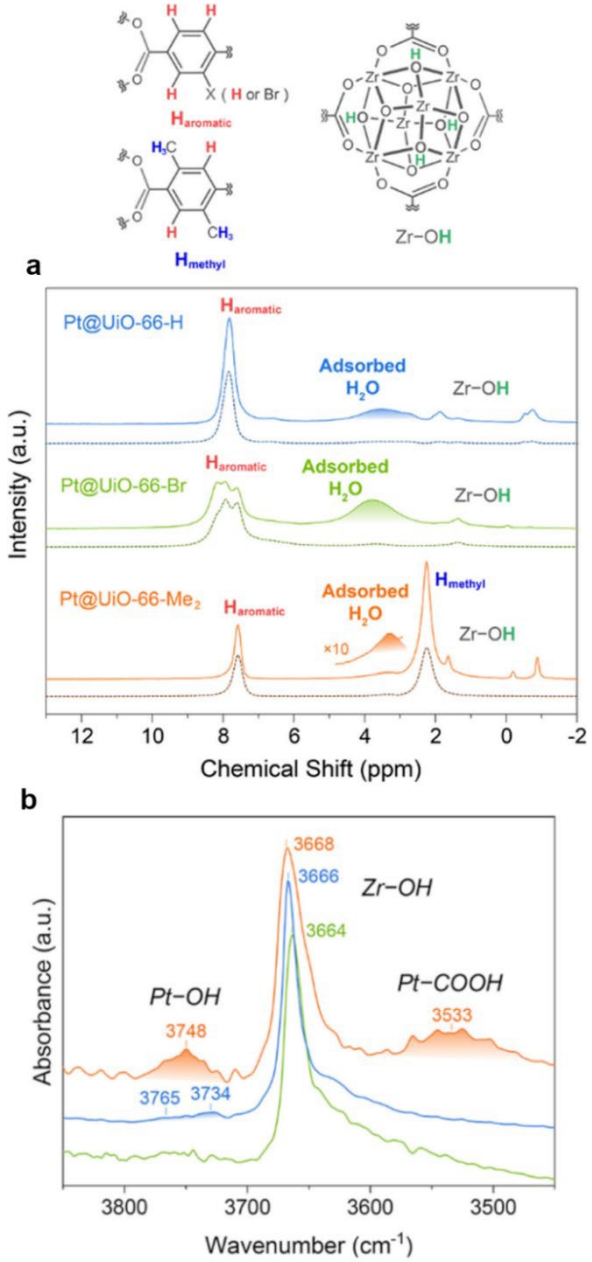

Fig. 9 (a) ^{1}H ultrafast (70 kHz) MAS NMR spectra (top, solid lines) and the corresponding ^{1}H-^{1}H double-quantum NMR (DQNMR) spectra (bottom, dashed lines) of Pt@UiO-66-H (blue), Pt@UiO-66-Br (green), and Pt@UiO-66-Me$_2$ (orange) at room temperature. The peaks attributed to adsorbed H_2O are highlighted. (b) In situ IR spectra on the condition of the WGS reaction for Pt@UiO-66-H (blue), Pt@UiO-66-Br (green), and Pt@UiO-66-Me$_2$ (orange). The gas flow rate was $H_2O/CO/N_2$ = 4.5/0.4/15.1 sccm, and the temperature was 300°C. Reprinted with permission from Ref 57. Copyright 2020 American Chemical Society.

3. 3. Electronic interactions between NPs and MOFs

In most cases, the electronic states of NPs play key roles in catalytic properties such as conversion and/or selectivity, and are affected by the properties of support materials. These phenomena can be observed in NP/MOF composite catalyst systems. The CO_2 hydrogenation to methanol reaction is one of the most intensively studied systems in NP/MOF composite catalysts because of the generally known structure sensitivity of the catalytic properties to the dimension and composition of the metal oxide−metal interface. The hybrid material of Cu NPs and Zr-based MOF, UiO-66, shows high activity and selectivity on CO_2 hydrogenation to methanol.[59] UiO-66 is one of the most intensively studied frameworks because of its high thermal, water, and chemical stabilities. In addition, it is easily functionalized through linker substitution[60] or defect formation,[61] making it more promising for electronic state control. Rungtaweevoranit *et al*. firstly reported that a catalyst composed of Cu NPs and UiO-66 (Cu⊂UiO-66) exhibits an 8-fold enhanced catalytic activity compared with the Al_2O_3-supported Cu catalyst.[59] From X-ray photoelectron spectroscopy (XPS) data, the authors suggested that Cu NPs and UiO-66 have strongly interacted because Zr(IV) in UiO-66 is reduced in the presence of Cu NPs (Fig. 10). The interface between Cu NPs and the Zr oxide cluster of UiO-66 was considered to be the active site for the composite catalyst.

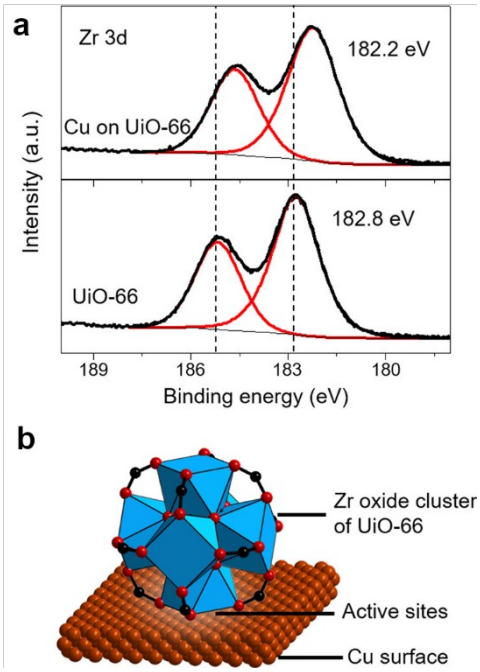

Fig. 10 (a) XPS spectra of UiO-66 before and after the hybridization with Cu NPs. (b) Illustration of the active point of Cu NP/UiO-66 catalyst. The brown, black, and red spheres represent the Cu, C, and O atoms, respectively. Zr is represented as blue polyhedra. H atoms are omitted for clarity. Reprinted with permission from Ref 59. Copyright 2016 American Chemical Society.

The effects of the electronic interaction between NPs and MOFs on the catalytic activity was further investigated by Kobayashi *et al*. [62] Cu/UiO-66 composite and different analogues, Cu/Zr-UiO-66, Cu/Zr-UiO-66-NH_2, Cu/Zr-UiO-66-COOH, and Cu/Hf-UiO-66 were synthesized to control the degree of charge transfer between Cu NPs and UiO-66. The composite catalysts were synthesized by the impregnation method. Copper acetylacetonate, $Cu(acac)_2$, was used as the metal precursor of the Cu NPs and it decomposed in the presence of the prepared MOF. From high-angle annular dark-field scanning TEM (HAADF-STEM) and energy-dispersive X-ray (EDX) elemental mappings, Cu NPs were confirmed to be covered with UiO-66 or its analogue. Cu/Zr-UiO-66 showed a high catalytic activity for CO_2 hydrogenation to methanol; the rate was larger by a factor of 70 than Cu/γ-Al_2O_3. The catalytic activities of Cu hybrid catalysts with other well-known MOFs such as ZIF-8 and MIL-100 were also investigated and they had poor CO_2 hydrogenation activities. To investigate the ligand substitution effect, the authors synthesized two different functionalized composite catalysts, Cu/Zr-UiO-66-COOH and Cu/Zr-UiO-66-NH_2. Carboxylate-functionalized Cu/Zr-UiO-66-COOH exhibited an enhancement of the rate of methanol synthesis by a factor of 3, whereas amine-functionalized Cu/Zr-UiO-66-NH_2 had almost the same catalytic activity as Cu/Zr-UiO-66. From the XPS measurement, it is considered that the charge transfer from Cu NPs to UiO-66 is a key factor in these enhancements of the catalytic activity of Cu. A clear correlation was found between the charge transfer and the catalytic activity (Fig. 11). Considering the changes in the oxidation state of Zr, the cationic Cu species due to charge transfer from Cu NPs to Zr in UiO-66 is thought to promote the CO_2 hydrogenation reaction. The cationic Cu species could stabilize formate, leading to the higher CO_2 hydrogenation activity because the hydrogenation of surface formate is the rate-limiting step.[63] In addition, the

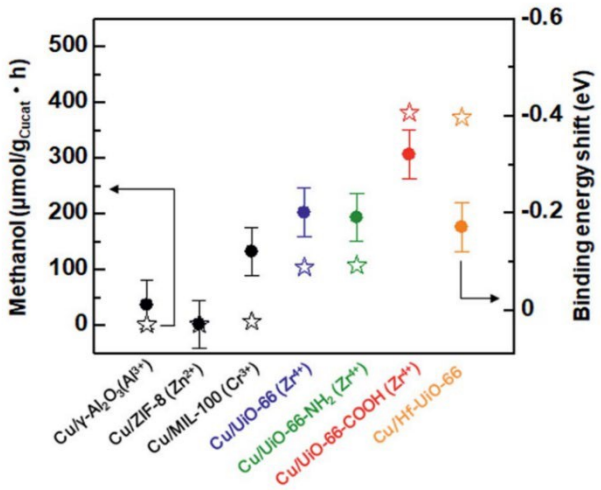

Fig. 11 Relationship between the catalytic activity and binding energy shift calculated from XPS analysis for Cu/γ-Al_2O_3 and Cu/MOF catalysts. Stars and circles represent synthesized methanol and binding energy shift, respectively. Reproduced from Ref. 62 with permission from the Royal Society of Chemistry.

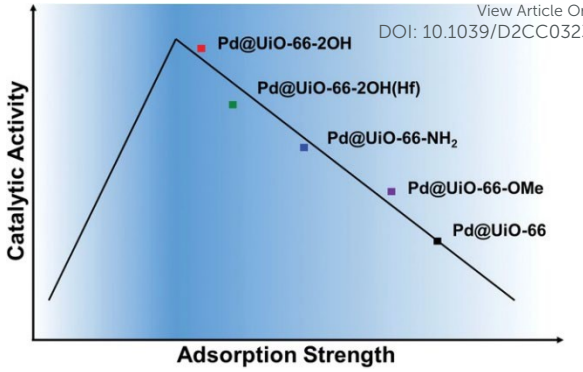

Fig. 12 Schematic plot of the relationship between adsorption strength and catalytic activity. Reproduced with permission from Ref. 64 Copyright 2020 Wiley-VCH.

component MOFs of the composite catalysts described above are crystalline; amorphous MOFs have also been reported to further enhance catalytic performance in CO_2 hydrogenation to methanol.[42]

The effect of ligand substitution on charge transfer between NPs and MOFs was also reported by Chen *et al*.[64] Pd NP@UiO-66-X (X = H, OMe, NH_2, OH, 2OH(Hf)) exhibited different catalytic activities in the hydrogenation of benzoic acid. Although all the catalysts presented nearly 100% selectivity, the catalytic activity followed the order of Pd@UiO-66-OH > Pd@UiO-66-2OH(Hf) > Pd@UiO-66-NH_2 > Pd@UiO-66OMe > Pd@UiO-66-H. From density functional theory (DFT) calculations, the numbers of electron transfers from Pd NPs to UiO-66-X changed according to the functional groups of the ligand or the MOF component metals (Zr or Hf), and their tendency was consistent with the catalytic activity. The differences in the surface electronic property of Pd NPs were also confirmed by the diffuse reflectance IR Fourier transform spectra of CO adsorption. The main adsorption peaks, assigned to the C–O vibrations of linearly adsorbed CO, exhibited red shift. This can be explained by the electron-donating property of functional groups on MOF ligands to the encapsulated Pd NPs; the order of electron donation degree was the reverse order of electron transfer numbers from DFT calculations. In addition, the position of the centre of the *d*-band states[65] of Pd NPs embedded in different UiO-66 analogues was also calculated. A higher *d*-band centre position brings a stronger interaction between the catalyst surface and the adsorbed molecule, as the occupancy of anti-bonding states becomes lower.[66,67] Hence, a higher *d*-band centre indicates a higher adsorption energy. Based on the *d*-band centre positions determined from the calculations, the order of adsorption energies (Pd@UiO-66-2OH < Pd@UiO-66-2OH(Hf) < Pd@UiO-66-NH_2 < Pd@UiO-66-OMe < Pd@UiO-66) was the reverse order of catalytic activity, and explains the experimental results well, considering the Sabatier principle (Fig. 12).[68]

Electronic interactions between metal NPs and MOFs also affect electrocatalytic activities. Wang *et al.* achieved oriented growth of NPs on MOF nanosheets (NSs) by controlling the reduction speeds of metal ions with different solvents.[69] They found that when weak reducing solvents such as ethylene glycol

and diethylene glycol were used, metal ions were reduced slowly and metal NPs grew selectively on the edge of pre-synthesized MOF NSs. By using this method, heterojunction composites of Pt NPs and MOF NSs (Pt/MOF-O) were fabricated and exhibited higher electrocatalytic activities for both alkaline and acidic hydrogen evolution reactions (HER). In contrast, composites of Pt NPs and MOF NSs with random distributions of NPs (Pt/MOF-C) showed lower HER activities than Pt/MOF-O, indicating that oriented growth of Pt NPs affects the catalytic performance. In the O 1s XPS spectra, a negative peak shift was observed in Pt/MOF-O, suggesting the electron-rich state of O in Pt/MOF-O (Fig. 13a). In contrast, no peak shift was observed in Pt/MOF-C. In the Pt 4f XPS spectra, Pt/MOF-O showed higher Pt^{2+}/Pt^{0} ratio than that of Pt/MOF-C. In addition, a peak attributed to C-O-Pt bonds was observed in the O 1s XPS spectrum of Pt/MOF-O. From these results, the authors concluded that the interaction between Pt NPs and MOFs occurred via C-O-Pt bonds and led to the electron transfer from Pt to O (Fig. 13c). Pt with low electron density is reported to promote electron transfer in the HER,[70] which may be a factor in the enhanced catalytic activity of Pt/MOF-O.

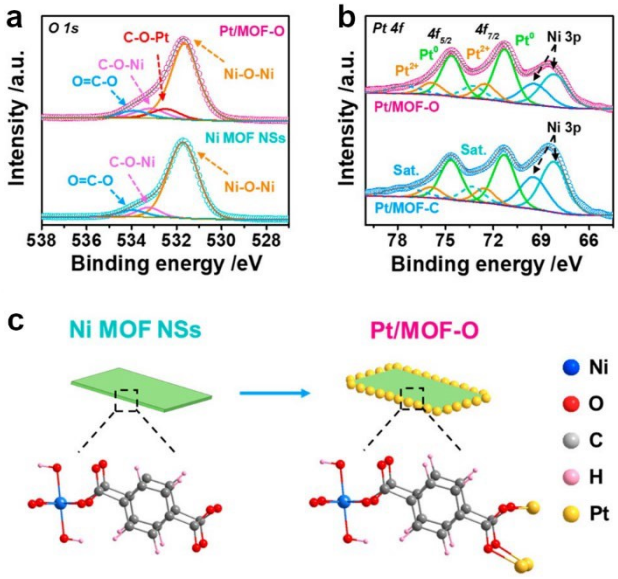

Fig. 13 (a) O 1s XPS spectra of Pt/MOF-O and Ni MOF NSs. (b) Pt 4f spectra of Pt/MOF-O and Pt/MOF-C. (c) Illustration showing the structure of Pt/MOF-O catalyst. Reprinted with permission from Ref 69. Copyright 2021 American Chemical Society.

3. 4. Other effects

As with other support materials such as zeolite and porous carbon, MOFs are reported to improve the stability of NPs by preventing their aggregation.[28,71] In particular, MOFs with regular and uniform cavities are advantageous in keeping small monodispersed NPs. Moreover, the tunability of MOF pore sizes can be used to control the size of NPs. For example, Mian *et al.* used two Zr-based MOFs, NU-901 and NU-907 with different pore diameters to control the size of embedded Cu NPs.[72] While both frameworks are composed of the same eight-connected Zr_6 nodes $[Zr_6(\mu_3\text{-}O)_4(\mu_3\text{-}OH)_4(H_2O)_4(OH)_4]$, their pore dimeters are different (15 Å and 10 Å) because the nodes are jointed by different linkers (1,3,6,8-tetrakis(*p*-benzoate)pyrene and 3,3',5,5'-azobenzenetetracarboxylic acid, respectively). Cu NPs were synthesized and embedded in the MOFs via wet impregnation method. Pair distribution function (PDF) analysis revealed that the particle size of the Cu NPs depends on the pore diameter of the host MOFs. In addition, Cu NPs@NU-901 exhibited higher activity than Cu NPs@NU-907 in acetylene semihydrogenation reaction. From DFT calculations, it was suggested that larger Cu NPs show higher activity, supporting their experimental results.

4. Conclusions and outlook

In this review, we reviewed the trends in NP/MOF hybrid catalysts, with a particular focus on elucidating the role of MOFs in catalysts. MOFs have many attractive properties in gas storage, separation, catalysis, and ion conduction, and their material development has extended to hybrid materials with other functional materials such as organic molecules, enzymes, polymers, metal NPs, and polyoxometalates. Among these composites, MOF composites with NPs have been intensively studied as a method for obtaining efficient catalysts. When they are hybridized with NPs, various functions of MOFs are suggested; examples include the molecular sieving, condensation, and electronic effects. To date, a variety of novel composite catalysts have been developed and some showed synergistic effects that resulted from interactions of NPs and MOFs. Significant efforts were made to develop NP/MOF hybrid materials; however, elucidation of the role of the MOFs in composite catalysts is still ongoing because multiple effects often occur simultaneously, making the analysis difficult.

Various synthetic methods for NP/MOF hybrid materials have been developed. We presented these techniques and classified them into three types: (1) the "bottle-around-ship approach", in which NPs are introduced into prepared MOFs, (2) the "ship-in-a-bottle", in which hybridization with a MOF occurs on prepared NPs, and (3) the one-pot method. In the bottle-around-ship approach, because of its simplicity, the solid grinding method was the earliest attempt to obtain these composites. The solution impregnation and CVD methods were developed as an outgrowth of the solid grinding method, and the former became one of the most popular preparation techniques. The self-template method also provides a facile way to obtain composite catalysts. The encapsulation method is also a popular technique and many researchers have used it. A disadvantage of the encapsulation method is the residue of NP protective agents, which acts as impurities; recently, a novel encapsulation method to achieve a direct interface between NPs and MOFs has been reported. Although there are only a few reports on this method, the one-pot method is an attractive technique when considering future practical applications.

We classified the effects to hybridize MOFs and NPs on the catalytic reaction, as follows. (1) Molecular sieving effects for reactant and/or product molecules, (2) interactions between reactant molecules and MOFs within the MOF pores, and (3)

electronic interactions between NPs and MOFs. MOFs are supposed to contribute to the activation of reactant molecules or regulation of NP surface properties, as the surface is the active site of the catalytic reactions. We introduced these synergistic effects of NP/MOF composite catalysts and attempts to elucidate the reaction mechanisms. The molecular sieving effects of MOFs have been reported in numerous reports and verified in various ways, including pore aperture control by ligand substitution. Affected by pore size and cavity flexibility, the type of reactants incorporated into the hybrid catalysts is controlled, and high catalytic activity and/or selectivity is achieved. In addition, interactions between reactants and MOFs are important factors to determine the catalytic properties of NP/MOF hybrid materials. MOFs are expected to condense and activate reactant molecules; however, in actual systems, diffusion effects compete, making the understanding of reaction mechanisms and following the design of composite catalysts difficult. The WGS reaction was taken as an example, to introduce the investigation of the reactivity of reactant molecules in MOFs. Competitive effects of condensation and diffusion in MOF pores were confirmed by testing composite catalysts with different preparation methods. Various analysis methods, including solid-state NMR and in situ IR measurement also demonstrated that the degree of activation of the reactants can be systematically tuned by functionalization of the MOF ligand. In addition, catalytic properties are significantly affected by the electronic states of NPs combined with MOFs. Although changes in the electronic structure of NPs upon hybridization with MOFs have been reported previously, as yet there is no systematic understanding on their catalytic performance. Recently, the ligand substitution effects of NP/MOF catalysts on catalytic activities were demonstrated and the degree of charge transfer between NPs and MOFs was shown to correlate with catalytic activity. The relationship between the electronic states of NPs in composite catalysts and catalytic performance has recently been discussed in terms of *d*-band centre theory.

To date, various efficient composite catalysts have been explored and developed; this style was investigated by the synthesis method and by tuning the MOF properties by ligand or metal substitution. However, the materials tend to date consist of limited combinations of platinum-group-metal NPs and well-known MOF frameworks (UiO-66 and ZIF-8). Furthermore, the development of facile synthetic methods and improvement of durability are also important factors for the practical use of NP/MOF catalysts. In particular, MOFs tend to have lower thermal stability than conventional support materials such as metal oxides and carbon materials, which is still one of big challenges. As mentioned in this review, elucidation of the reaction mechanisms in NP/MOF catalysts is still in the process of development. We believe further development of analytical techniques will provide guidelines for novel catalyst design and broaden the scope of exploration.

Conflicts of interest

There are no conflicts to declare.

Acknowledgements

View Article Online
DOI: 10.1039/D2CC03233C

The authors acknowledge the support of JSPS KAKENHI Grant-in-Aid for Specially Promoted Research (20H05623).

Notes and references

1 O. M. Yaghi, M. O'Keeffe, N. W. Ockwig, H. K. Chae, M. Eddaoudi and H. K. Chae, *Nature*, 2003, **423**, 705–714.
2 S. Kitagawa, R. Kitaura and S.-I. Noro, *Angew. Chem. Int. Ed.*, 2004, **43**, 2334–2375.
3 H. Furukawa, K. E. Cordova, M. O'Keeffe and O. M. Yaghi, *Science*, 2013, **341**, 1230444.
4 M. Eddaoudi, J. Kim, N. Rosi, D. Vodak, J. Wachter, M. O'Keeffe and O. M. Yaghi, *Science*, 2002, **295**, 469–472.
5 J.-R. Li, R. J. Kuppler and H.-C. Zhou, *Chem. Soc. Rev.*, 2009, **38**, 1477–1504.
6 J. Lee, O. K. Farha, J. Roberts, K. A. Scheidt, S. T. Nguyen and J. T. Hupp, *Chem. Soc. Rev.*, 2009, **38**, 1450–1459.
7 M. Sadakiyo and H. Kitagawa, *Dalton Trans.*, 2021, **50**, 5385–5397.
8 C.-Y. Sun, S.-X. Liu, D.-D. Liang, K.-Z. Shao, Y.-H. Ren and Z.-M. Su, *J. Am. Chem. Soc.*, 2009, **131**, 1883–1888.
9 J. Liu, T. A. Goetjen, Q. Wang, J. G. Knapp, M. C. Wasson, Y. Yang, Z. H. Syed, M. Delferro, J. M. Notestein, O. K. Farha and J. T. Hupp, *Chem. Soc. Rev.*, , DOI:10.1039/D1CS00968K.
10 Y. Shen, T. Pan, L. Wang, Z. Ren, W. Zhang and F. Huo, *Adv. Mater.*, , DOI:10.1002/adma.202007442.
11 H. Zhang, X. Liu, Y. Wu, C. Guan, A. K. Cheetham and J. Wang, *Chem. Commun.*, 2018, **54**, 5268–5288.
12 Y.-S. Wei, M. Zhang, R. Zou and Q. Xu, *Chem. Rev.*, 2020, **120**, 12089–12174.
13 U. Olsbye, S. Svelle, M. Bjørgen, P. Beato, T. V. W. Janssens, F. Joensen, S. Bordiga and K. P. Lillerud, *Angew. Chem. Int. Ed.*, 2012, **51**, 5810–5831.
14 F. Rodríguez-reinoso, *Carbon*, 1998, **36**, 159–175.
15 S. Hermes, M.-K. Schröter, R. Schmid, L. Khodeir, M. Muhler, A. Tissler, R. W. Fischer and R. A. Fischer, *Angew. Chem. Int. Ed.*, 2005, **44**, 6237–6241.
16 T. Ishida, M. Nagaoka, T. Akita and M. Haruta, *Chem. Eur. J.*, 2008, **14**, 8456–8460.
17 P. Hu, J. V. Morabito and C.-K. Tsung, *ACS Catal.*, 2014, **4**, 4409–4419.
18 Q. Yang, Q. Xu and H.-L. Jiang, *Chem. Soc. Rev.*, 2017, **46**, 4774–4808.
19 M. Zhao, K. Deng, L. He, Y. Liu, G. Li, H. Zhao and Z. Tang, *J. Am. Chem. Soc.*, 2014, **136**, 1738–1741.
20 L. He, Y. Liu, J. Liu, Y. Xiong, J. Zheng, Y. Liu and Z. Tang, *Angew. Chem. Int. Ed.*, 2013, **52**, 3741–3745.
21 H.-L. Jiang, B. Liu, T. Akita, M. Haruta, H. Sakurai and Q. Xu, *J. Am. Chem. Soc.*, 2009, **131**, 11302–11303.
22 H. R. Moon, J. H. Kim and M. P. Suh, *Angew. Chem. Int. Ed.*, 2005, **44**, 1261–1265.
23 J. K. Sun, W. W. Zhan, T. Akita and Q. Xu, *J. Am. Chem. Soc.*, 2015, **137**, 7063–7066.
24 M. Samy El-Shall, V. Abdelsayed, A. El Rahman S. Khder, H. M. A. Hassan, H. M. El-Kaderi and T. E. Reich, *J. Mater. Chem.*, 2009, **19**, 7625–7631.
25 A. K. Singh and Q. Xu, *ChemCatChem*, 2013, **5**, 3000–3004.
26 Q.-L. Zhu, J. Li and Q. Xu, *J. Am. Chem. Soc.*, 2013, **135**, 10210–10213.
27 N. Ogiwara, H. Kobayashi, P. Concepción, F. Rey and H. Kitagawa, *Angew. Chem. Int. Ed.*, 2019, **58**, 11731–11736.
28 A. Aijaz, A. Karkamkar, Y. J. Choi, N. Tsumori, E. Rönnebro, T. Autrey, H. Shioyama and Q. Xu, *J. Am. Chem. Soc.*, 2012, **134**, 13926–13929.

29 F. Schröder, D. Esken, M. Cokoja, M. W. E. van den Berg, O. I. Lebedev, G. Van Tendeloo, B. Walaszek, G. Buntkowsky, H.-H. Limbach, B. Chaudret and R. A. Fischer, *J. Am. Chem. Soc.*, 2008, **130**, 6119–6130.

30 M. Mukoyoshi, H. Kobayashi, K. Kusada, M. Hayashi, T. Yamada, M. Maesato, J. M. Taylor, Y. Kubota, K. Kato, M. Takata, T. Yamamoto, S. Matsumura and H. Kitagawa, *Chem. Commun.* , 2015, **51**, 12463–12466.

31 Y. Fu, X. Zhai, S. Wang, L. Shao, X.-J. Bai, Z.-S. Su, Y.-L. Liu, L.-Y. Zhang and J.-Y. Chen, *Inorg. Chem.*, 2021, **60**, 16447–16454.

32 L. Chen, H. Chen, R. Luque and Y. Li, *Chem. Sci.*, 2014, **5**, 3708–3714.

33 T. Tsuruoka, H. Kawasaki, H. Nawafune and K. Akamatsu, *ACS Applied Materials & Interfaces*, 2011, **3**, 3788–3791.

34 G. Lu, S. Li, Z. Guo, O. K. Farha, B. G. Hauser, X. Qi, Y. Wang, X. Wang, S. Han, X. Liu, J. S. DuChene, H. Zhang, Q. Zhang, X. Chen, J. Ma, S. C. J. Loo, W. D. Wei, Y. Yang, J. T. Hupp and F. Huo, *Nat. Chem.*, 2012, **4**, 310–316.

35 G. Li, H. Kobayashi, J. M. Taylor, R. Ikeda, Y. Kubota, K. Kato, M. Takata, T. Yamamoto, S. Toh, S. Matsumura and H. Kitagawa, *Nat. Mater.*, 2014, **13**, 802–806.

36 Y. Li, W.-S. Lo, F. Zhang, X. Si, L.-Y. Chou, X.-Y. Liu, B. P. Williams, Y.-H. Li, S.-H. Jung, Y.-S. Hsu, F.-S. Liao, F.-K. Shieh, M. N. Ismail, W. Huang and C.-K. Tsung, *J. Am. Chem. Soc.*, 2021, **143**, 5182–5190.

37 C.-H. Kuo, Y. Tang, L.-Y. Chou, B. T. Sneed, C. N. Brodsky, Z. Zhao and C.-K. Tsung, *J. Am. Chem. Soc.*, 2012, **134**, 14345–14348.

38 T. Friscić, D. G. Reid, I. Halasz, R. S. Stein, R. E. Dinnebier and M. J. Duer, *Angew. Chem. Int. Ed.*, 2010, **49**, 712–715.

39 S. Tanaka, K. Kida, T. Nagaoka, T. Ota and Y. Miyake, *Chem. Commun.* , 2013, **49**, 7884–7886.

40 X. Li, Z. Zhang, W. Xiao, S. Deng, C. Chen and N. Zhang, *J. Mater. Chem. A*, 2019, **7**, 14504–14509.

41 H. Kobayashi, Y. Mitsuka and H. Kitagawa, *Inorg. Chem.*, 2016, **55**, 7301–7310.

42 Y. Mitsuka, N. Ogiwara, M. Mukoyoshi, H. Kitagawa, T. Yamamoto, T. Toriyama, S. Matsumura, M. Haneda, S. Kawaguchi, Y. Kubota and H. Kobayashi, *Angew. Chem. Int. Ed.*, 2021, **60**, 22283–22288.

43 K. M. Choi, K. Na, G. A. Somorjai and O. M. Yaghi, *J. Am. Chem. Soc.*, 2015, **137**, 7810–7816.

44 J. H. Cavka, S. Jakobsen, U. Olsbye, N. Guillou, C. Lamberti, S. Bordiga and K. P. Lillerud, *J. Am. Chem. Soc.*, 2008, **130**, 13850–13851.

45 W. Zhang, G. Lu, C. Cui, Y. Liu, S. Li, W. Yan, C. Xing, Y. R. Chi, Y. Yang and F. Huo, *Adv. Mater.*, 2014, **26**, 4056–4060.

46 C. J. Stephenson, J. T. Hupp and O. K. Farha, *Inorg. Chem.*, 2016, **55**, 1361–1363.

47 L. Chen, W. Zhan, H. Fang, Z. Cao, C. Yuan, Z. Xie, Q. Kuang and L. Zheng, *Chem. Eur. J.*, 2017, **23**, 11397–11403.

48 D. Fairen-Jimenez, S. A. Moggach, M. T. Wharmby, P. A. Wright, S. Parsons and T. Düren, *J. Am. Chem. Soc.*, 2011, **133**, 8900–8902.

49 W. Morris, B. Leung, H. Furukawa, O. K. Yaghi, N. He, H. Hayashi, Y. Houndonougbo, M. Asta, B. B. Laird and O. M. Yaghi, *J. Am. Chem. Soc.*, 2010, **132**, 11006–11008.

50 Z. Li, R. Yu, J. Huang, Y. Shi, D. Zhang, X. Zhong, D. Wang, Y. Wu and Y. Li, *Nat. Commun.*, 2015, **6**, 8248.

51 H. K. Lee, Y. H. Lee, J. V. Morabito, Y. Liu, C. S. L. Koh, I. Y. Phang, S. Pedireddy, X. Han, L.-Y. Chou, C.-K. Tsung and X. Y. Ling, *J. Am. Chem. Soc.*, 2017, **139**, 11513–11518.

52 K. Na, K. M. Choi, O. M. Yaghi and G. A. Somorjai, *Nano Lett.*, 2014, **14**, 5979–5983.

53 F. Stallmach, S. Gröger, V. Künzel, J. Kärger, O. M. Yaghi, M. Hesse and U. Müller, *Angew. Chem. Int. Ed.*, 2006, **45**, 2123–2126.

54 Q. Yang, W. Liu, B. Wang, W. Zhang, X. Zeng, C. Zhang, Y. Qin, X. Sun, T. Wu, J. Liu, F. Huo and J. Lu, *Nat. Commun.*, 2017, **8**, 14429.

55 S. Navarro-Jaén, M. Á. Centeno, O. H. Laguna and J. A. Odriozola, *J. Mater. Chem. A*, 2018, **6**, 17001–17010.

56 L. C. Grabow, A. A. Gokhale, S. T. Evans, J. A. Dumesic and M. Mavrikakis, *J. Phys. Chem. C*, 2008, **112**, 4608–4617.

57 N. Ogiwara, H. Kobayashi, M. Inukai, Y. Nishiyama, P. Concepción, F. Rey and H. Kitagawa, *Nano Lett.*, 2020, **20**, 426–432.

58 G. S. Karlberg and G. Wahnström, *Phys. Rev. Lett.*, 2004, **92**, 136103.

59 B. Rungtaweevoranit, J. Baek, J. R. Araujo, B. S. Archanjo, K. M. Choi, O. M. Yaghi and G. A. Somorjai, *Nano Lett.*, 2016, **16**, 7645–7649.

60 S. Biswas and P. Van Der Voort, *Eur. J. Inorg. Chem.*, 2013, **2013**, 2154–2160.

61 H. Wu, Y. S. Chua, V. Krungleviciute, M. Tyagi, P. Chen, T. Yildirim and W. Zhou, *J. Am. Chem. Soc.*, 2013, **135**, 10525–10532.

62 H. Kobayashi, J. M. Taylor, Y. Mitsuka, N. Ogiwara, T. Yamamoto, T. Toriyama, S. Matsumura and H. Kitagawa, *Chem. Sci.*, 2019, **10**, 3289–3294.

63 Y. Yang, C. A. Mims, D. H. Mei, C. H. F. Peden and C. T. Campbell, *J. Catal.*, 2013, **298**, 10–17.

64 D. Chen, W. Yang, L. Jiao, L. Li, S.-H. Yu and H.-L. Jiang, *Adv. Mater.*, 2020, **32**, e2000041.

65 B. Hammer and J. K. Nørskov, *Surf. Sci.*, 1995, **343**, 211–220.

66 B. Hammer and J. K. Nørskov, in *Advances in Catalysis*, Academic Press, 2000, vol. 45, pp. 71–129.

67 H. Xu, D. Cheng, D. Cao and X. C. Zeng, *Nature Catalysis*, 2018, **1**, 339–348.

68 A. J. Medford, A. Vojvodic, J. S. Hummelshøj, J. Voss, F. Abild-Pedersen, F. Studt, T. Bligaard, A. Nilsson and J. K. Nørskov, *J. Catal.*, 2015, **328**, 36–42.

69 M. Wang, Y. Xu, C.-K. Peng, S.-Y. Chen, Y.-G. Lin, Z. Hu, L. Sun, S. Ding, C.-W. Pao, Q. Shao and X. Huang, *J. Am. Chem. Soc.*, 2021, **143**, 16512–16518.

70 F.-Y. Yu, Z.-L. Lang, L.-Y. Yin, K. Feng, Y.-J. Xia, H.-Q. Tan, H.-T. Zhu, J. Zhong, Z.-H. Kang and Y.-G. Li, *Nat. Commun.*, 2020, **11**, 490.

71 D. Esken, S. Turner, O. I. Lebedev, G. Van Tendeloo and R. A. Fischer, *Chem. Mater.*, 2010, **22**, 6393–6401.

72 M. R. Mian, L. R. Redfern, S. Pratik, D. Ray, J. Liu, K. B. Idrees, T. Islamoglu, L. Gagliardi and O. K. Farha, *Chem. Mater.*, 2020, **32**, 3078–3086.